Weak radiative decay $\Lambda \rightarrow n\gamma$ and the radiative capture reaction $K^- p \rightarrow \Sigma(1385)\gamma$

K. D. Larson,[h,*] A. J. Noble,[c,†] B. Bassalleck,[h] H. Burkhardt,[i] W. J. Fickinger,[e] J. R. Hall,[h] A. L. Hallin,[j,‡] M. D. Hasinoff,[c] D. Horvath,[f,k] P. G. Jones,[a] J. Lowe,[a,h] E. K. McIntyre,[b,§] D. F. Measday,[c] J. P. Miller,[b] B. L. Roberts,[b] D. K. Robinson,[e] M. Sakitt,[d] M. Salomon,[k] S. Stanislaus,[c,g] C. E. Waltham,[c] T. M. Warner,[b,**] D. A. Whitehouse,[b,g] and D. M. Wolfe[h]

[a]*University of Birmingham, Birmingham, B15 2TT, United Kingdom*
[b]*Boston University, Boston, Massachusetts 02215*
[c]*University of British Columbia, Vancouver, British Columbia, Canada V6T 1Z1*
[d]*Brookhaven National Laboratory, Upton, New York 11973*
[e]*Case Western Reserve University, Cleveland, Ohio 44106*
[f]*Central Research Institute for Physics, H-1525 Budapest, Hungary*
[g]*Los Alamos Meson Physics Facility, Los Alamos, New Mexico 87545*
[h]*University of New Mexico, Albuquerque, New Mexico 87131*
[i]*University of Nottingham, Nottingham, NG7 2RD, United Kingdom*
[j]*Princeton University, Princeton, New Jersey 08544*
[k]*TRIUMF, Vancouver, British Columbia, Canada, V6T 2A3*

(Received 22 May 1992)

The branching ratio for the Λ weak radiative decay $\Lambda \rightarrow n\gamma$ has been measured. Three statistically independent results from the same experiment (Brookhaven E811) are reported here. They are combined with a previously published measurement, also from Brookhaven E811, to yield a result of $(\Lambda \rightarrow n\gamma)/(\Lambda \rightarrow \text{anything}) = (1.75 \pm 0.15) \times 10^{-3}$, based on 1800 events after background subtraction. This represents a factor of 75 increase in statistics over the previous world total. A comparison with recent theoretical papers shows that no existing model provides a completely satisfactory description of all data on weak radiative decays. A search is also reported for the radiative capture process $K^- p \rightarrow \Sigma(1385)\gamma$ at rest. No signal was observed and an upper limit on the branching ratio of $[K^- p \rightarrow \Sigma(1385)\gamma]/[K^- p \rightarrow \text{anything}] < 4 \times 10^{-4}$ (90% C.L.) was determined.

PACS number(s): 13.40.Hq, 13.75.Jz, 14.20.Jn

I. INTRODUCTION

Apart from the electromagnetic decay $\Sigma^0 \rightarrow \Lambda\gamma$, nonleptonic decays of hyperons are of two types: the pionic decays of the form $B_1 \rightarrow B_2 + \pi$ and the weak radiative decays $B_1 \rightarrow B_2 + \gamma$. The study of pionic decays has the experimental advantage of a relatively large branching ratio, but their interpretation involves more complicating strong-interaction effects than the weak radiative decays. Weak radiative decays involve both a weak and an electromagnetic vertex, but have no strong interaction in the final state. Since photon emission is better understood theoretically than pion emission, weak radiative decays should enable the nonleptonic weak vertex to be examined in detail. Unfortunately, theories attempting to describe the hyperonic weak radiative decays have encountered difficulties. One manifestation of these difficulties is the experimentally observed [1–4] large negative asymmetry (for polarized Σ's) in the decay $\Sigma^+ \rightarrow p\gamma$. This asymmetry is in the proton direction with respect to the spin of the Σ. In the limit of exact $SU(3)_f$, this asymmetry vanishes. Since $SU(3)_f$ is known to be broken at a small level, the experimentally observed magnitude of this asymmetry, in the range of -0.7 to -0.8, is indeed surprising. To date, no theoretical model has been able to account for this asymmetry and at the same time predict the branching ratios of all the weak radiative decays with any acceptable degree of accuracy.

Prior to the present experiment, the branching ratio for the process $\Lambda \rightarrow n\gamma$ had been measured only once, by Biagi *et al.* [5]. Although no clear signal was observed, a branching ratio was extracted from their data based on 23.7 candidate events. The experiment described in the present paper has observed a clear weak radiative decay signal above the background, and has obtained almost two orders of magnitude more $\Lambda \rightarrow n\gamma$ events than had been observed previously.

This paper presents the last phase of Brookhaven National Laboratory experiment E811, which studied a number of rare processes following the capture of a K^- on a proton or deuteron. Over a period of four years, in addition to the results reported here, E811 has measured the branching ratio for the weak radiative decay [6,7] $\Sigma^+ \rightarrow p\gamma$ as well as for the radiative capture processes

*Present address: Center for Naval Analyses, Alexandria, VA 22302.
†Present address: PPE Division, CERN, CH-1211 Geneva 23, Switzerland.
‡Present address: Queens University, Kingston, Ontario, Canada K7L 3N6.
§Present address: Eaton Corporation, Beverly, MA 01915.
**Present address: Department of Chemistry, University of California Berkeley, Berkeley, CA 94720.

[8–11] $K^-p\to\Lambda\gamma$, $K^-p\to\Sigma^0\gamma$, and $K^-d\to\Lambda n\gamma$.

The experiment was designed to stop kaons in a liquid-hydrogen (LH_2) target. This produced Λ hyperons through two different processes. In the first process, $K^-p\to\Lambda\pi^0$ ($B=6.7\%$) [12,13]. Since the π^0 decays quickly to two γ's, the decay $\Lambda\to n\gamma$ would result in a three-γ event. The other process that produced Λ hyperons was $K^-p\to\Sigma^0\pi^0$ ($B=27.3\%$), $\Sigma^0\to\Lambda\gamma$ ($B=100\%$). In this case, the $\Lambda\to n\gamma$ decay results in a 4-γ event. The principal decay modes of the Λ are $\Lambda\to p\pi^-$ ($B=64.1\%$) and $\Lambda\to n\pi^0$ ($B=35.7\%$) [13]. The first of these two was rejected in hardware by charged-particle veto counters described later, while the second was used as a normalization to arrive at a final branching ratio for $\Lambda\to n\gamma$. The 3- and 4-γ results were analyzed separately, and the results from each of these analyses will be presented.

Although the direct production channel $K^-p\to\Lambda\pi^0$ does not produce polarized Λ's, it has been shown by Düsedau and Jaffe [14] that polarized Λ's can be produced from the interference of the two amplitudes: $K^-p\to\pi^0\Sigma^0\to\pi^0\Lambda\gamma$ and $K^-p\to\Sigma(1385)\gamma\to\pi^0\Lambda\gamma$. The calculated polarization reached a maximum of 30% depending on the branching ratio for the radiative capture $K^-p\to\Sigma(1385)\gamma$. To explore the possibility of obtaining a sample of polarized Λ's, we have looked for this radiative capture, since its observation is essential to tagging polarized Λ production.

The search for this radiative capture reaction fit well with the first phase of E811. In fact, the radiative capture processes $K^-p\to Y\gamma$ for kaons at rest have attracted considerable attention for some time [15–18]. The interest results mainly from the proximity of the mass of the K^-p system at rest (1432 MeV) to that of the $\Lambda(1405)$, which has a width of $\sim$40 MeV. Thus the K^-p system at rest is strongly influenced by the $\Lambda(1405)$ and this reaction provides an opportunity to study its properties [19]. The $\Lambda(1405)$ is a poorly understood object, and its interpretation as either a three-quark state or as a $\bar{K}N$ bound state has a long history of uncertainty [19–21]. The series of radiative capture measurements in earlier phases of the present experiment is continued here in a search for the capture channel $K^-p\to\Sigma(1385)\gamma$ at rest. No signal was observed for this process, but an upper limit was determined.

The data taking took place in two phases. The first phase consisted of a test run in the spring of 1988, followed by a main data-taking run in 1989. Because of a longer period of stable running and an improved data acquisition system, the 1989 run acquired several times more candidate events than the 1988 test, allowing the application of tighter cuts on the data. Although primarily intended to study the performance of the apparatus, the test run provided a sample of useful data, and a result from the 3-γ events from this run has been published already [22]. The present paper describes the experiment in more detail and reports on the analysis of all data from both runs.

II. THEORIES OF WEAK RADIATIVE DECAY

The two essential quantities to be measured and calculated for these decays are the branching ratio and the decay asymmetry. The matrix element for the transition

$$B_i(P_i)\to B_f(P_f)+\gamma(k)\ ,\quad k=P_i-P_f$$

is typically written as

$$M=iG_Fe\bar{u}_f(P_f)(a+b\gamma_5)\sigma_{\mu\nu}k^\nu u_i(P_i)\epsilon^\mu\ .$$

Here a and b represent the parity-conserving (p-wave) and parity-violating (s-wave) terms, respectively. The decay rate then becomes

$$\Gamma=\pi^{-1}G_F^2e^2\left[\frac{m_i^2-m_f^2}{2m_i}\right]^3(|a|^2+|b|^2)\ ,$$

and the asymmetry parameter

$$\alpha_\gamma=\frac{2\,\mathrm{Re}(a^*b)}{|a|^2+|b|^2}\ .$$

This asymmetry parameter describes the decay γ angular distribution relative to the initial hyperon spin. For polarized hyperons one finds an angular distribution of the form

$$I(\theta)=c(1+\alpha_\gamma P\cos\theta)\ ,$$

where P is the initial hyperon polarization and θ is the angle between the final-state baryon momentum and the hyperon spin. It was the unexpectedly large and negative asymmetry for $\Sigma^+\to p\gamma(\alpha_\gamma=-0.7$ to $-0.8)$ that confounded theorists, since standard weak-interaction models predicted α_γ to be zero, at least in the SU(3) limit [23]. Getting all the branching ratios *and* all the asymmetries consistent with experiment has remained a theoretical challenge.

Many different theoretical approaches, both at the baryon and at the quark level, have been employed over the years. We list here some recent references and refer the reader to the references cited therein for all the earlier work: combined SU(6) symmetry and vector-dominance approach [24]; combined $\Delta I=\frac{1}{2},\Delta S=1$ quark Hamiltonian [25]; short- and long-distance contributions to the nonleptonic weak Hamiltonian [26]; Bethe-Salpeter formalism [27]; QCD sum-rule approaches [28]; Pole models [29]; PCAC (partial conservation of axial-vector current) and correlations between radiative and pionic decays [30]; single- and two-quark transitions in a constituent quark model [31]; Skyrme model [32]; effective quark-gluon-photon operator [33]; MIT bag model [34]; and SU(6)-broken quark-diquark model [35].

With the advent of the Glashow-Salam-Weinberg model, attempts have been made at the quark level to explain these weak radiative hyperon decays. A variety of "spectator" and "nonspectator" quark diagrams (or equivalently, one-quark, two-quark, and three-quark diagrams) can contribute to such processes. We summarize these quark diagrams in Fig. 1. The consensus from a comparison between theory and experiment seems to be that all these diagrams contribute, and that none of them is dominant. It is worth pointing out that the two- and three-quark diagrams of Fig. 1 cannot contribute to the Ξ^- and Ω^- weak radiative decays because these two hyperons do not contain any valence u quarks.

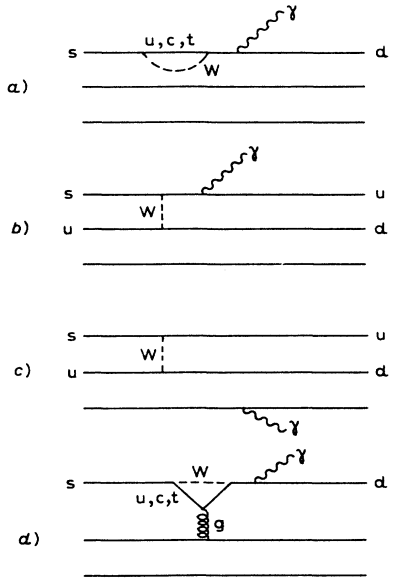

FIG. 1. Quark diagrams for weak radiative decays, including one-quark (a), two-quark (b), three-quark (c), and the so-called penguin diagram (d).

A review of recent theoretical and experimental work on weak radiative decays has been given by Bassalleck [36]. A comparison of our branching ratio result for $\Lambda \rightarrow n\gamma$ with different theoretical models will be given in Sec. VI A.

III. APPARATUS

Experiment E811 was performed at BNL in the low-energy separated beam LESB II of the Alternating Gradient Synchrotron (AGS). Under normal AGS running conditions, beam spills lasting about 1.5 s were extracted every 2.8 s. Typically, a spill of $2-3\times10^{12}$ protons resulted in a beam of about 6×10^{4} kaons with a π/K ratio of about 6–7. Kaon beam momenta of 600 and 680 MeV/c were used.

The beam entered the experimental area through a lead collimator and passed through the beam-line counters shown in Fig. 2. Beam kaons and pions were identified via a coincidence of the counters $S1\times S2\times S3\times S4$ and with the Lucite Čerenkov counters K and C. The dE/dx counters $E1$ and $E2$ (labeled E in Fig. 2) served a dual purpose. They helped to discriminate between beam kaons and pions as well as to suppress high-momentum kaons that would not stop in the LH_2 target. The hodoscope H, shown in Fig. 2, was composed of twelve 2.54-cm-wide and 0.32-cm-thick scintillators, six in each direction transverse to the beam. Its information was used to reconstruct the event vertex position with about 3-cm position resolution in each transverse direction (x and y). No z vertex information was available from the hodoscope, nor was an attempt made to extract such information from the dE/dx counters.

The spherical LH_2 target was mounted in an evacuated cylindrical cryostat. The walls of the cryostat were constructed to be as thin as possible to minimize interactions between them and the outgoing γ's. The center of the target was surveyed to coincide with the center of our detector, the Crystal Box.

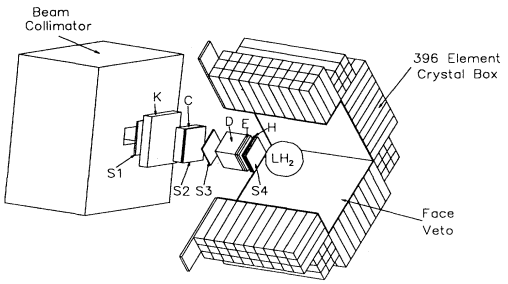

FIG. 2. Layout of the apparatus showing the main detectors and the target. A cutaway view of the Crystal Box is shown. The octagonal veto counter surrounding the target is omitted for clarity.

The Crystal Box calorimeter is a NaI(Tl) detector array [37,38] constructed at the Los Alamos Meson Physics Facility (LAMPF). The detector consists of 396 optically isolated NaI(Tl) crystals, 360 of which are $6.35\times6.35\times30.5$ cm grouped into 4 faces of 90 crystals each. These four faces are oriented transverse to the beam as shown in Fig. 2. The remaining 36 crystals measure $6.35\times6.35\times76.2$ cm and are grouped into 4 corners of 9 crystals each. These corner crystals were oriented along the beam direction as shown in Fig. 2. Each NaI(Tl) crystal was mounted within a single sealed aluminum housing. The Crystal Box was used in this experiment because of its large solid-angle coverage (about 2π sr), its efficiency, and its resolution for measuring high-energy photons. References [37,38] give more information on the construction and performance of the Crystal Box.

Signals from the Crystal Box elements were clipped to reduce pileup, and split so that the prompt part of the signals could be summed in hardware to provide a measure of the total energy in the Crystal Box. The delayed signals were further subdivided and fed to both the main analogue-to-digital converters (ADC's) and to the "pile-up" ADC's. The main ADC's were gated with a 250-ns pulse, while the pileup ADC's were gated with a 50-ns gate, sampling the 25 ns prior to the event trigger and the first 25 ns of the data signal. During analysis, piled-up pulses were rejected by imposing a condition that the pulses in each pair of ADC's have the correct ratio.

Since the experiment involved recording only events with all neutral particles in the final state, two layers of scintillators were installed to veto any event containing a charged particle in the final state. The first layer of veto counters consisted of eight separate 0.3-cm-thick scintillators arranged in the form of an octagon surrounding the LH_2 target within the cryostat. The octagon was open at the upstream end to allow beam particles to enter the target. Four of the eight scintillators were bent over to close off the downstream end of the octagon to aid in detecting particles which did not stop in the LH_2 target.

In addition to the octagon veto, the four faces of the Crystal Box were covered with two sets of veto counters. The 0.6-cm-thick face veto counters covered the surface of each of the four faces between the LH_2 target and the NaI(Tl) crystals. These counters were thick enough to detect the passage of most charged particles but thin enough to allow γ's of interest to pass through with a very low probability of converting. The 2.54-cm-thick guard counters covered the upstream side of each quadrant of the Crystal Box. The purpose of these guard counters was to protect the Crystal Box from beam-related halo or secondary particles.

A beam kaon was defined by $K_{\text{beam}} \equiv S1 \times S2 \times S3 \times S4 \times \bar{C} \times E1 \times E2 \times K$. $\bar{C}$ indicates that no signal was present from the Čerenkov detector (no pion was present), K indicates that a beam kaon was detected in the velocity selecting ("Fitch") Čerenkov counter, while $E1$ and $E2$ indicate that the appropriate amount of energy was deposited in these dE/dx counters. In addition to requiring a beam-related kaon, the hardware trigger required the event to contain only neutral particles in the final state. This was indicated when none of the face or octagon counters detected the passage of a charged particle. The hardware trigger for data events also required at least 300 MeV to be deposited in the Crystal Box and a beam-on gate from the AGS.

The Crystal Box was calibrated by stopping π^- in the LH_2 target and using the monoenergetic photopeak at 129.4 MeV from $\pi^- p \rightarrow n\gamma$. The resolution obtained for this peak varied from 7% (FWHM) for central crystals of a face to 11% (FWHM) for corner crystals. A pion beam around 240 MeV/c was used for these calibrations. Additional information was also derived from the π^0 box resulting from the stopped π^- reaction $\pi^- p \rightarrow \pi^0 n$. The range of γ energies from this π^0 box is $54.9 \leq E_\gamma \leq 83.0$ MeV. A beam pion was defined in hardware as $\pi_{\text{beam}} \equiv S1 \times S2 \times S3 \times S4 \times \bar{C} \times E1 \times E2$, where here $\bar{C}$ indicates that no electron was present. These calibration events required different discriminator thresholds as well as a lower total energy requirement (≥ 40 MeV).

In an effort to minimize gain drifts due to temperature variations in the experimental area, a temperature control system was constructed for the Crystal Box. The Crystal Box was encased in a Herculite enclosure. A system consisting of a heater and several fans kept the temperature of the Crystal Box at 28.5 ± 1.5 °C. The temperature of the Crystal Box was written to tape once every beam spill using a thermistor circuit read by an ADC. The temperature control system is described in detail in Ref. [39]. Over the course of several months the gain drift for the majority of crystals amounted to only a few percent.

A xenon flasher system was used to track the gains of individual crystals between calibration runs. Each phototube light guide of the crystal box had a fiber optic cable that connected it to the xenon flasher. The flasher system was triggered by a pulser at a rate of about 1 Hz.

The data acquisition system was designed to distribute the required tasks for acquiring the data to a multilayered command structure in hardware. A Digital Equipment Corporation PDP 11/44 was used as the data acquisition computer. It ran the LAMPF Q data acquisition system. The PDP 11 communicated with a BiRa MBD/11 microprogrammable branch driver that supervised one of the CAMAC branches.

The next layer of intelligence consisted of a LeCroy CAMAC booster (CAB), branch driver (BG), and crate controller (CG). The CAB BG supervised a second CAMAC branch containing LeCroy fast encoding and readout ADC's (4300-B FERA's).

Tasks were distributed among the various components of the system to increase the speed of data acquisition. The system was capable of accomplishing up to three independent tasks simultaneously. For example, the MBD might be reading out one CAB BG memory module while a FERA system was filling another, all while the CAB codes continued their internal bookkeeping.

Further details of the experimental setup are given in Refs. [39,40].

IV. PROCEDURE

The experiment ran for about 4 weeks during the 1988 test run and 12 weeks during the main data-taking run in 1989. Several times during the running periods gain calibration runs were carried out using the stopped π^- beam.

During the 1988 test run, a study of degrader materials was made by employing copper, high-density graphite, and BeO. Pure copper was found to give the best ratio of stopping kaons to high-energy background. The thickness of the degrader was adjusted to maximize the number of kaons stopping in the LH_2 target.

During the 1989 run, pedestal subtraction and sparse readout were used in the FERA ADC's. Since pedestals were subtracted in hardware, it was important to supply the FERA's with accurate pedestal information. Pedestal events were triggered by a pulser, and pedestal runs were taken every 1–2 days during the running period. The pedestals were checked for both beam on and beam off; no change was observed, and the beam-off events were used to calculate the pedestals. Pedestal values were found to be very stable throughout the running period.

The data compression due to pedestal subtraction lowered the system dead time from ~40% in the 1988 run to ~10% during the 1989 running. The maximum data acquisition rate using this system was about 400 data events of 150–200 words each, per beam spill. All data were written to magnetic tape for offline analysis.

Finally, some runs were taken with liquid deuterium in the target and with a stopping π^- beam. This produced neutrons through the reactions

$$\pi^- d \rightarrow nn\gamma \ , \quad \pi^- d \rightarrow nn \ ,$$

and the data from these runs were used to study neutron interactions in the Crystal Box.

V. DATA ANALYSIS

In order to provide a check on the analysis process, the data sets from the 1988 and 1989 runs were analyzed separately at different laboratories. The two analysis efforts proceeded independently up to the point where prelimi-

nary results were available. The two independent analyses provided valuable checks on the analysis methods and the physics assumptions.

All phases of the data analysis utilized a modified version of MOLLI, a code developed at TRIUMF. This software searched the Crystal Box for energy groupings or "clumps." Each clump represented the energy deposited by a γ or neutron, and the location of where the particle entered the Crystal Box.

Clumps were located by searching for the crystal containing the most energy, the high-pulse-height crystal (HPHC). To this was added all of the energy in this crystal's neighborhood set, the group of crystals close to the HPHC, typically including the two rows of columns of crystals surrounding the HPHC. All crystals whose energy was added into a clump were labeled as being used for each event so that this energy would not be used again in some future clump for the same event.

This procedure of locating the HPHC and adding to it the energy in that crystal's neighborhood set was continued until the last remaining HPHC contained less than 5 MeV of energy. The method was developed at LAMPF [37,38], and the procedure used here is similar to the one used at LAMPF except for some minor changes in the neighborhood set definitions. These changes were indicated upon examination of shower distribution in both data and simulated events, and are described in detail in Refs. [39,40].

Finding the γ energies in this way has some limitations. For example, if two γ's entered the Crystal Box so close together that the HPHC of one γ was contained in the neighborhood set of another, the software may divide the energy wrongly between the two γ's and may even fail to recognize the existence of the second. Different approaches to this problem were used in analysis of the two data sets. For the 1988 data, the energy contained in each overlapping crystal was shared between the two clumps. This division was weighted according to the proximity of the overlapping crystal to the HPHC, and to the energy of the respective clumps. The weighting factors were determined experimentally from examination of clean single-γ clumps. Since the 1989 data set contained many more events, a more cautious view was taken; events were rejected when it appeared possible that errors might be introduced by overlapping of clumps. To do this, a cut was imposed on the rms size of each clump. Monte Carlo studies proved that this quantity is usually much larger for clumps containing γ's that overlap. In addition, for the 1989 data set, if the neighborhood sets of two HPHC's overlapped and any overlapping crystal contained more than 2 MeV, the event was rejected. These cuts reduced the problem of overlapping clumps to the point where it could be reliably calculated in the Monte Carlo simulation.

Another problem is that the total clump energy is always less than the real γ energy due to energy leakage from the sides and back of crystals in the Crystal Box. The extent of this leakage depends upon the proximity of the clump to an edge of the Crystal Box. This problem was corrected by observing the shift in total energy of the monoenergetic $\pi^- p \to n\gamma$ gamma (129.4 MeV). The shift in γ energy was dependent upon the location of the HPHC, and the energy of each clump was corrected according to this shift to yield the true γ energy.

As an additional precaution against excessive shower leakage, the event was rejected if crystals on the upstream and downstream edges of the Crystal Box and outside corner crystals were clump HPHC's. Furthermore, if any edge or outside corner crystal was not an HPHC but still contained more than 50 MeV, the event was rejected in the 1989 data set.

The Crystal Box has some sensitivity to neutrons. It is expected that a neutron interacting in the NaI will leave most of its energy in a single element of the crystal box. During the analysis, it was assumed that any clump in which more than 95% of the clump energy was in a single crystal resulted from a neutron.

Experimental studies were made to determine the neutron detection efficiency and also the effectiveness of this $>95\%$ single-crystal energy cut in identifying a neutron. These studies used neutron signals from the process $K^- p \to \Lambda\pi^0$, $\Lambda \to n\pi^0$ and also from $K^- p \to \Sigma^- \pi^+, \Sigma^- \to n\pi^-$. In addition, data from $\pi^- d \to nn$ and $nn\gamma$ were used. For neutrons of kinetic energy ~ 60 MeV, the detection efficiency was found to be about 30% for a clump energy threshold of 10 MeV, but only $\sim 6\%$ when the threshold was raised to 25 MeV. The efficiency variation with clump threshold energy is reasonably consistent with the observed pulse-height spectrum from neutron interactions. The $>95\%$ energy criterion was found to be less satisfactory. It is correct only 22% of the time for a threshold of 10 MeV and 50% of the time for a threshold of 25 MeV. Since the maximum neutron energy is well below the signal γ energy, wrongly identified neutron clumps cannot give a background in the signal region. They are unlikely to be mistaken for a π^0-decay γ because of the tight cut on the π^0 mass. If a neutron clump is misidentified, a genuine event could be lost because the multiplicity would be counted wrongly. However, this amounts to $<2\%$ of events and affects both signal and normalization channels by the same factor. In the end the neutron information was not used in the analysis.

Although charged-particle events were vetoed in hardware, the possibility existed for a charged event immediately preceding a valid event trigger, since these events were very prolific. Since the charged-particle event could leave unwanted residual light in the Crystal Box, any event that was preceded by a charged event (as detected by the face veto counters), by up to 450 ns prior to the event trigger, was rejected.

Since the required beam intensities were relatively high, signal pileup was a definite concern. The signals from each NaI detector element of the crystal box were sent to two ADC's, as described earlier. The ratio of these ADC's could then be used to eliminate signal pileup.

A. Simulation

Two independent simulation programs were used in the course of the analysis. This was partly to maintain the independence of the analyses of the two data sets, but

more importantly to take account of the different requirements of the two analyses.

The first simulation program used in analysis of the 1988 data set, was based on the CERN GEANT 3.13 package, interfaced to GHEISHA [41]. This was used to generate events in the LH_2 target and to track the resulting particles and γ's through the target walls and veto counters into the NaI of the crystal box. The development of the electromagnetic shower in the NaI was also modeled. This procedure gives a realistic simulation of the experiment, but has the disadvantage of requiring a large amount of computing time.

The other program used, KPSPEC, was used for the 1989 data set. It generated events in much the same way as GEANT and followed the reaction products out into the NaI. Some approximations were used in this calculation. However, the principal limitation of this program was that the shower development in the NaI was not calculated. Instead, the empirically determined line shape for the Crystal Box was folded into the energy spectrum of γ's reaching the NaI to give the simulated spectrum shape.

In general, each of these simulation programs was found to give reasonable agreement with the data for γ's, but the treatment for neutrons was less satisfactory. GEANT predicts a neutron detection efficiency of $\sim 40\%$ for a threshold of 10 MeV, which is in reasonable agreement with $30\pm 10\%$ found experimentally (see above). However, GEANT calculations suggest that neutron interactions should nearly always leave $\geq 95\%$ of the total deposited energy in a single NaI crystal. This does not agree well with the experimental numbers quoted above. Since the KPSPEC program does not follow the shower development in the NaI, it cannot make predictions about the shower development or neutron detection efficiency.

B. Analysis of $\Lambda \rightarrow n\gamma$: 3-$\gamma$ events

The most promising channel to look at for the decay $\Lambda \rightarrow n\gamma$ is the stopped reaction $K^- p \rightarrow \Lambda\pi^0$ followed by $\Lambda \rightarrow n\gamma$, where the π^0 decays promptly into two γ's. Since the reaction takes place at rest, the π^0 is a monoenergetic at 287.8 MeV. These events were selected by requiring two of the three γ's to reconstruct to a π^0 with tight cuts on the π^0 energy, momentum, and invariant mass. Figure 3 shows the energy spectrum of π^0's; signals for $K^- p \rightarrow \Lambda\pi^0$ and $K^- p \rightarrow \Sigma^0\pi^0$ are clearly visible.

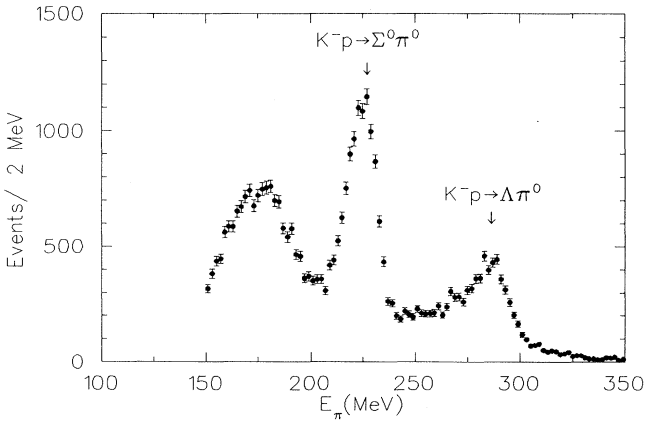

FIG. 3. Energy spectrum of π^0's from $K^- p$ interactions.

Unfortunately, the in-flight process $K^0 p \rightarrow \bar{K}^0 n$ followed by $\bar{K}^0 \rightarrow \pi^0\pi^0$ can be a significant background process if one of the π^0's passes the energy and momentum cuts, while one γ from the other π^0 misses the Crystal Box. These events were largely eliminated by using a cut on the angle between the reconstructed direction of the Λ and the direction of the candidate weak radiative decay γ, $\Theta_{\Lambda\gamma}$. By isolating events where two π^0's reconstructed a $\bar{K}^0$ in the data, it was determined that limiting $\Theta_{\Lambda\gamma}$ to values greater than about 90° virtually eliminated this background in the signal region; however, this also resulted in a significant loss of data events. The $\Theta_{\Lambda\gamma}$ distribution for 3-γ events is shown in Fig. 4. Also shown are the simulation predictions for all events and for the $K^- p \rightarrow \bar{K}^0 n$ channel, showing the effectiveness of this cut.

The channels included in the simulation were

(a) $K^- p \rightarrow \Lambda\pi^0$, $\Lambda \rightarrow n\pi^0$,
(b) $K^- p \rightarrow \Sigma^0\pi^0$, $\Sigma^0 \rightarrow \Lambda\gamma$, $\Lambda \rightarrow n\pi^0$,
(c) $K^- p \rightarrow \Lambda\gamma$, $\Lambda \rightarrow n\pi^0$,
(d) $K^- p \rightarrow \Lambda\pi^0$, $\Lambda \rightarrow n\gamma$, and
(e) $K^- p \rightarrow \bar{K}^0 n$, $\bar{K}^0 \rightarrow \pi^0\pi^0$.

Channels (a)–(d) were calculated for K^- at rest and also for K^- in flight. Channel (e) has a threshold at 89 MeV/c, so it occurs only for in-flight interactions. The kaon momentum spectrum for in-flight interactions in the present experimental setup was calculated in Refs. [8,10]. A broad distribution was found, centered at about 225 MeV/c. The distribution was represented for the present analysis by a Gaussian centered at this momentum.

The following parameters were varied in the fit: (i) the contribution from channels (a)–(c) for kaon interactions at rest; (ii) the contribution from the signal channel (d); (iii) the contributions from all channels (a)–(e) for kaon interactions in flight; (iv) the energy calibration parame-

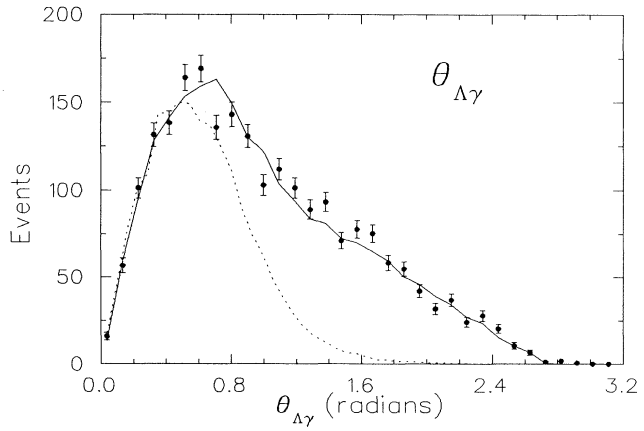

FIG. 4. Distribution of the Λ decay angle $\Theta_{\Lambda\gamma}$ for a sample of the data. The curves show predictions of the simulation program, the solid line for all events and the dotted line for the channel $K^- p \rightarrow \bar{K}^0 n$ only.

ter of the Crystal Box. The relative contributions of channels (a)–(c) for kaon interactions at rest were held fixed at values taken from the Particle Data Group tables [13], and the relative contributions for (a)–(c) and (e) for in-flight kaons were fixed at values estimated from the known cross sections [42]. The energy calibration parameter for the Crystal Box was varied to allow for minor gain changes between the calibration runs and the data taking. The resulting shift was about 0.2%.

The experimental spectrum from the 1989 data, together with the fit, is shown in Fig. 5. A dominant feature of the spectrum is the "box" resulting from the decay of the π^0 in the stopped process $K^- p \to \Lambda\pi^0, \Lambda \to n\pi^0$, where one of the γ's from the π^0 in the Λ decay has missed the Crystal Box. The energy range of the other is $33.2 \le E_\gamma \le 137.1$ MeV. The small peak visible at 74 MeV is due to the γ from the decay $\Sigma^0 \to \Lambda\gamma$, produced by the background process $K^0 p \to \Sigma^0\pi^0, \Sigma^0 \to \Lambda\gamma, \Lambda \to n\pi^0$, when one γ from each of the π^0's showers into the Crystal Box in a way that mimics a 288-MeV π^0, and the other two γ's from the π^0's miss the Crystal Box. An enlargement of the interesting region is shown in Fig. 5(b). In the Λ rest frame, the weak radiative decay γ is monoenergetic at 162.2 MeV; this is shown as a dotted line.

The χ^2 and number of degrees of freedom for the fit are given in Table I. Although the χ^2 is somewhat higher than the number of degrees of freedom, almost all of this comes from the high-energy edge of the π^0 "box" at $E_\gamma \sim 120$ MeV. In this region, the Monte Carlo prediction is quite sensitive to the details of the γ-ray line shape, and small errors in the tails of the Crystal Box response function can give a large contribution to χ^2. In the signal region, at $E_\gamma \sim 162$ MeV, the contribution to the background from high-energy tails of lower-energy γ's is negligible; the background here arises from other physics channels. The fit in the signal region is adequately good, and the somewhat high χ^2 at $E_\gamma \sim 120$ MeV does not reflect any inadequacy in simulation in the signal region.

The branching ratio was calculated using the known branching ratio for the reaction $\Lambda \to n + \pi^0$ ($B = 35.7 \pm 0.5\%$) for normalization in the following way:

$$B\left[\frac{\Lambda \to n+\gamma}{\Lambda \to \text{all}}\right] = B\left[\frac{\Lambda \to n+\gamma}{\Lambda \to n+\pi^0}\right] B\left[\frac{\Lambda \to n+\pi^0}{\Lambda \to \text{all}}\right],$$

where the ratio $B[(\Lambda \to n+\gamma)/(\Lambda \to n+\pi^0)]$ is determined by fitting the Monte Carlo calculation to the data.

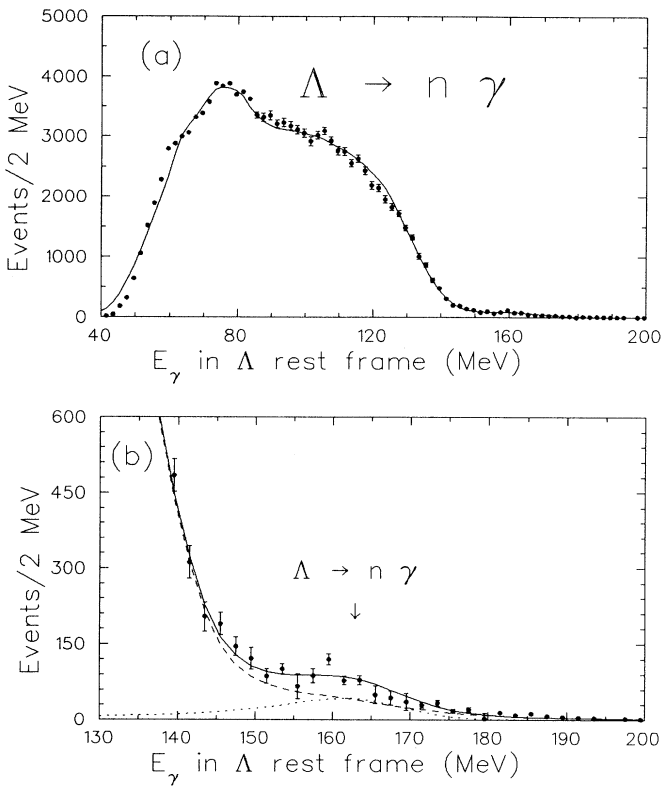

FIG. 5. Spectrum of candidate γ's in the Λ rest frame for $\Lambda \to n\gamma$ from 3-γ events for the 1989 data. The solid curve is the fitted simulation prediction. In plot (b), the dotted curve is the fitted signal contribution and the dashed curve is the sum of contributions from all other channels.

This method is advantageous since the efficiencies of most of the cuts that were used are the same for the $\Lambda \to n + \gamma$ channel as they are for the $\Lambda \to n + \pi^0$ channel (where one of the π^0 γ's has missed the Crystal Box), so that these effects cancel in the ratio. An exception to this is the $\Theta_{\Lambda\gamma}$ cut, where the different efficiencies are corrected for using the Monte Carlo calculation. The results of the 3-γ analysis for the 1989 data are shown in Table I.

Results for the 3-γ channel for the 1988 data have already been published [22]. The analyses of the 1988 and 1989 data used similar methods, differing mainly in the use of generally tighter cuts in the 1989 data analysis. The only significant difference in the analysis procedure was in the determination of the fraction of kaons in-

TABLE I. Branching ratios for $\Lambda \to n\gamma$ from the present experiment. For each branching ratio, the first error quoted is from the fitting to the simulation (including statistical error) and the second is the systematic error. The χ^2 and number of degrees of freedom for the fit are also given.

Data set	Event type	Branching ratio	Number of events	χ^2	Degrees of freedom
1988	3-γ	$(1.78 \pm 0.24^{+0.14}_{-0.16}) \times 10^{-3}$	287	98	78
1988	4-γ	$(1.68 \pm 0.49 \pm 0.52) \times 10^{-3}$	252	140	120
1989	3-γ	$(1.74 \pm 0.18 \pm 0.10) \times 10^{-3}$	546	144	112
1989	4-γ	$(1.72 \pm 0.18 \pm 0.35) \times 10^{-3}$	731	158	62

teracting in flight; in the 1988 data this was derived from a study of the $\bar{K}^0 n$ events, while in the 1989 data the in-flight contribution was varied in the fit.

C. Analysis of $\Lambda \to n\gamma$: 4-γ events

Extraction of the $\Lambda \to n\gamma$ decay from the 4-γ events proceeded in a similar fashion to the 3-γ analysis described above. The signal channel is now $K^- p \to \Sigma^0 \pi^0$, $\Sigma^0 \to \Lambda\gamma$, $\Lambda \to n\gamma$. Again, the decay γ was transformed to the Λ rest frame, and the signal should appear as a 162.2-MeV monoenergetic γ in this frame. This source of $\Lambda \to n\gamma$ events was more difficult to analyze for two reasons.

(i) Since the $K^- p$ atom decay energy is distributed among four rather than three γ's, the average γ energy is lower. A serious background therefore results from the channel $K^- p \to \Lambda\pi^0, \Lambda \to n\pi^0$, which gives four γ's of similar average energy to those from the signal channel and gives a broad distribution in the region of the signal γ.

(ii) Because of the lower average γ energy, the Monte Carlo prediction was more sensitive to neutron clumps misidentified as γ's in the Crystal Box. As mentioned above, neutrons are not well described by the simulation. In the analysis of the 1988 data, neutron signals were eliminated completely by imposing a lower limit of 62 MeV on all clumps in the analysis. This cut was not used in analysis of the 1989 data.

A compensating advantage of the 4-γ channel is that the average Λ momentum is lower. Thus the Doppler shift between the laboratory and Λ rest frames is less, resulting in a slightly narrower signal line in the Λ rest frame.

Because of the above problems, the branching ratios extracted from the 4-γ events are subject to larger systematic errors than the 3-γ results. The 4-γ results served as a consistency check on the analysis procedures, and they are also included in the final average of all data sets.

Cuts were imposed on the π^0 mass, the π^0 energy, the energy of the decay γ from $\Sigma^0 \to \Lambda\gamma$, and the decay angle $\Theta_{\Lambda\gamma}$ of the Λ. One additional cut was used in analysis of the 1988 data. In addition to requiring that the two γ's from the π^0 decay had the invariant mass of a π^0, it was also required that other γ pairs did not. This cut gave some reduction in the background from $K^- p \to \Lambda\pi^0, \Lambda \to n\pi^0$, although with an appreciable loss of genuine events.

Apart from detailed differences in the cuts selected, the analyses of the 1988 and 1989 4-γ data sets differed in two significant respects. First was the use of a GEANT simulation for the 1988 data and a KPSPEC simulation for the 1989 data. The second difference concerned the normalization of the contribution from in-flight interactions. Since there is no exact way of calculating the magnitude or shape of the momentum spectrum of kaon interactions in flight, for the 1989 data set, both the magnitude and the shape were treated as variable parameters in the fit. For the 1988 data set, an attempt was made to derive an independent estimate of the in-flight contributions by isolating events from the process $K^- p \to \bar{K}^0 n, K_S^0 \to \pi^0\pi^0$ which can only occur in flight. The contribution from this channel is strongly suppressed in the analysis by the cut on $\Theta_{\Lambda\gamma}$, but by temporarily removing this cut the channel can be clearly identified and can be used to estimate the magnitude of the in-flight interactions. The procedure is described in detail for 3-γ events in Ref. [22].

The fitted spectra for the 4-γ events from the 1988 and 1989 data sets are shown in Figs. 6 and 7. The channels included in the simulation were the same as channels (a)–(e) used in fitting the 3-γ data, except that channel (d) was replaced by the signal channel for 4-γ events, $K^- p \to \Sigma^0 \pi^0$, $\Sigma^0 \to \Lambda\gamma, \Lambda \to n\gamma$. Since the low-energy events were removed at an early stage in the analysis, only the high-energy part of the π^0 box appears in the spectrum; hence the fitting was confined to the region above 110 MeV. The fits yielded the branching ratios given in Table I. As for the 3-γ events, the χ^2 (given in Table I) is dominated by the edge of the π^0 box, and the fit is good in the signal region, at $E_\gamma \sim 162$ MeV. The χ^2 for the 1989 data is particularly affected by the cutoff at ~ 110 MeV.

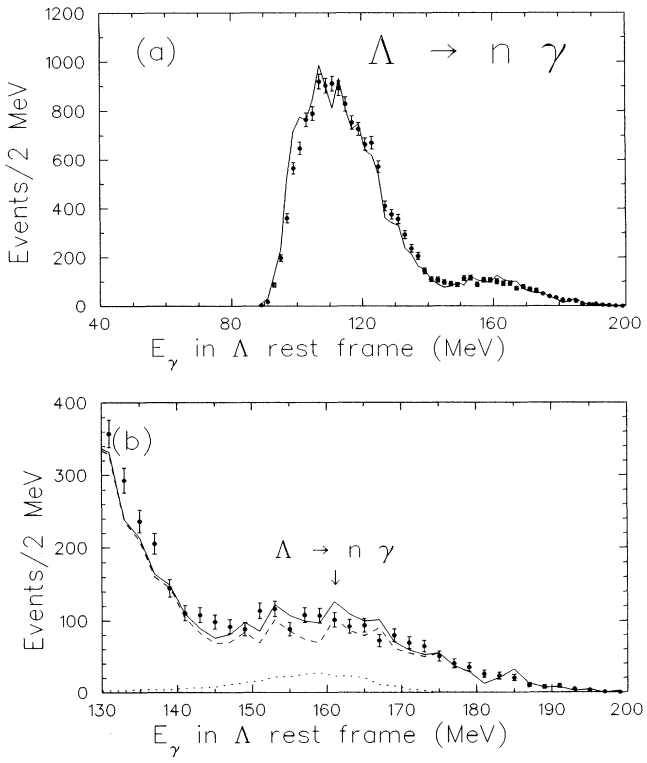

FIG. 6. Spectrum of candidate γ's in the Λ rest frame for $\Lambda \to n\gamma$ from 4-γ events for the 1988 data. The solid curve is the fitted simulation prediction. In plot (b), the dotted curve is the fitted signal contribution and the dashed curve is the sum of contributions from all other channels.

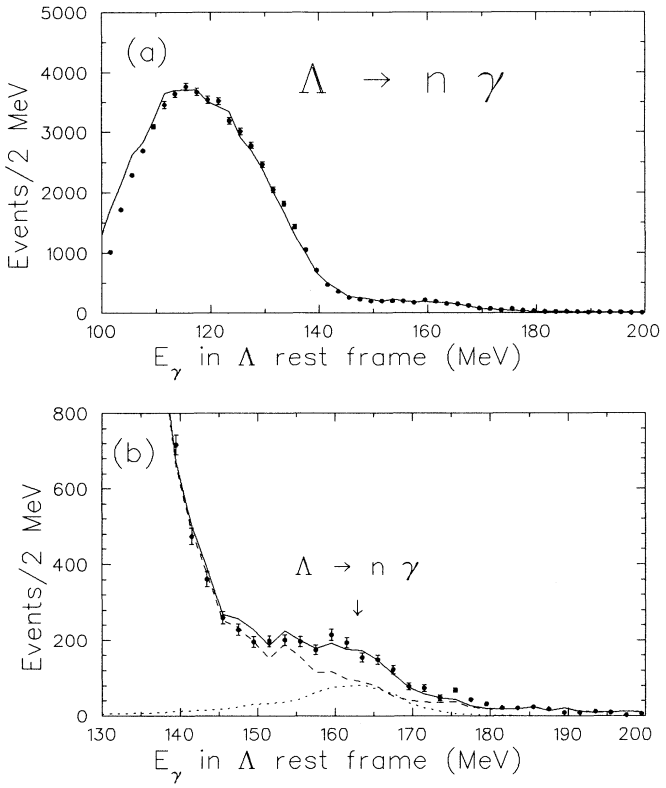

FIG. 7. Spectrum of candidate γ's in the Λ rest frame for $\Lambda \to n\gamma$ from 4-γ events for the 1989 data. The solid curve is the fitted simulation prediction. In plot (b), the dotted curve is the fitted signal contribution and the dashed curve is the sum of contributions from all other channels.

D. Analysis of the radiative capture $K^- p \to \Sigma(1385)\gamma$

The radiative capture at rest, $K^- p \to \Sigma(1385)\gamma$, gives a 5-$\gamma$ signal by the process

$$\text{(a)}\ K^- p \to \Sigma(1385)\gamma\ ,\ \Sigma(1385) \to \Lambda\pi_1^0(88\%)\ ,$$
$$\Lambda \to n\pi_2^0(36\%)\ ,$$

with $\pi^0 \to \gamma\gamma$. The capture γ has a mean energy of 47 MeV. However, it is not monoenergetic but is broadened substantially by the width (36 MeV) of the $\Sigma(1385)$.

The only other significant source of 5-γ events is the process

$$\text{(b)}\ K^- p \to \Sigma^0\pi_1^0(27\%)\ ,\ \Sigma^0 \to \Lambda\gamma(100\%)\ ,$$
$$\Lambda \to n\pi_2^0(36\%)\ .$$

This is substantially more prolific than the expected rate for the radiative capture process, and hence, it forms the main contribution to the background.

Each of these processes involve two π^0's together with a fifth γ (not associated with a π^0), and these have fairly similar energies in the two processes. The following differences were used to search for process (a) in the presence of the background process (b).

(i) The laboratory energy of π_1^0 is centered around 248 MeV in process (a) and is monoenergetic at 226 MeV in process (b).

(ii) The laboratory energy of the fifth γ for process (a) is 47 MeV, broadened by the width of the $\Sigma(1385)$. For process (b) the energy of the γ is monoenergetic in the Σ rest frame at 74 MeV.

(iii) The angle between π_1^0 and the fifth γ shows a peak at small angles for process (a) but not for process (b).

Cuts based on these differences were then applied to the data for all 5-γ events. In addition, the following cuts were applied.

(iv) The missing mass of the event was required to be the neutron mass.

(v) The invariant mass of the Λ and π_1^0 corresponds to the $\Sigma(1385)$ mass.

(vi) The invariant mass of the Λ and the fifth γ *does not* correspond to that of the Σ.

(vii) The invariant mass of the fifth γ and any of the four γ's attributed to π^0 decay *does not* correspond to that of a π^0.

If the cuts (i)–(vii) are set to select (rather than reject) the background process (b), then this process dominates the resulting sample of events. This is illustrated in Fig. 8, which shows the 74-MeV γ from the decay $\Sigma^0 \to \Lambda\gamma$ in the Σ^0 rest frame. This signal, together with the acceptances for processes (a) and (b) from the simulation program, was used to normalize the radiative capture branching ratio.

With the cuts set to select process (a) and reject process (b), the spectrum of Fig. 9 results. The 74-MeV γ is now absent, and most of the remaining events are in the region of the radiative capture γ. The simulation prediction for the radiative capture γ is also shown in the figure. Almost no simulation events for the background process (b) survive the cuts. Nevertheless, the events in Fig. 9 cannot reliably be ascribed to radiative capture. This is partly because background events might pass the cuts if they involve the tails of energy and angle distributions which are not handled very well by the simulation program and cannot adequately be tested experimentally.

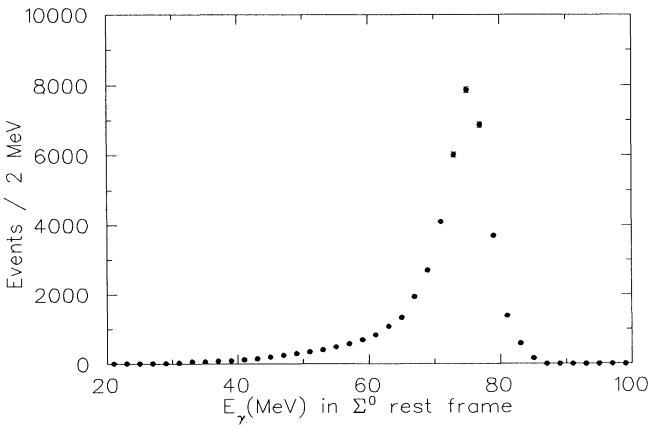

FIG. 8. Spectrum of candidate γ's for $\Sigma^0 \to \Lambda\gamma$ in the Σ^0 rest frame. A monoenergetic γ at 74 MeV is expected.

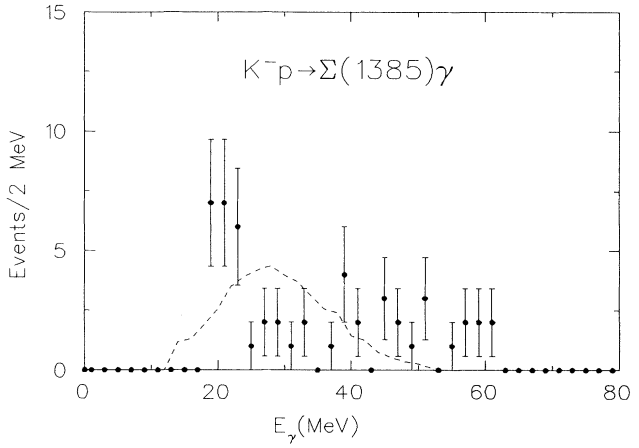

FIG. 9. Spectrum of candidate γ's for $K^-p \to \Sigma(1385)\gamma$ from 5-γ events. The curve shows the simulation prediction for this channel. It is peaked below the nominal 47 MeV because of a cut on the energy of π^0_1.

In addition, the distribution in the spectrum does not match the simulation very well for radiative capture. Indeed, the spectrum of experimental events could be ascribed to the tail of the 74-MeV γ together with a contribution from background γ's and neutrons at low energies. Therefore, we take a more cautious approach; if *all* the events in Fig. 9 in the range $24 < E_\gamma < 40$ MeV are attributed to process (a), this gives an upper limit on the signal contribution. The resulting branching ratio is

$$\frac{K^-p \to \Sigma(1385)\gamma}{K^-p \to \text{anything}} < 4 \times 10^{-4} \quad (90\%\ \text{C.L.}) .$$

VI. DISCUSSION

A. The weak radiative decay $\Lambda \to n\gamma$

Table I shows the three results for the Λ weak radiative decay branching ratio found here, together with the result already published from the present experiment [22], that from 3-γ events in the 1988 data. The first errors quoted result from fitting the spectra with the simulation output and contain the statistical errors. Systematic errors arise from many sources, but the most important are the effect of small variations in the cuts used and in the region of the spectra fitted, uncertainties in the target-empty subtraction and in the in-flight contribution, and the effects of possible inefficiencies in the veto counters. In addition, the 4-γ result is sensitive to the ratio $(K^-p \to \Sigma^0\pi^0)/(K^-p \to \Lambda\pi^0)$, so uncertainties in this ratio contribute to systematic errors in the 4-γ result.

Table I shows that the four results are in good agreement. The four results were combined to yield an average branching ratio. In doing so, due allowance was made for the fact that the systematic error due to uncertainties in the K^-p atom branching ratios affect both 4-γ results in the same way (though it is negligible for the 3-γ results). Although other sources of systematic error affect all results in a given data set in the same way, their effect is different from one data set to another, so they are combined in quadrature with the statistical errors. The final weighted average is

$$B\left[\frac{\Lambda \to n\gamma}{\Lambda \to \text{anything}}\right] = (1.75 \pm 0.15) \times 10^{-3} .$$

This result is based on 1816 weak radiative decay events, about $\frac{2}{3}$ of which lie in the peak region and so influence the fit quite significantly.

The present result is about 2.0 standard deviations higher than that from the only previously published experiment, that of Biagi *et al.* [5], which found a branching ratio of $(1.02 \pm 0.33) \times 10^{-3}$. Their method was very different from ours, and their result is based on just 24 events. A comparison of the two methods is given by Noble *et al.* [22], where it is suggested that, apart from the limited statistics in the experiment of Biagi *et al.*, the difference may result from an incomplete simulation of the liquid-argon calorimeter used in their experiment.

In Ref. [22] we have already compared our 1988 3-γ result with a representative sample of theoretical results. Our conclusion was that although our branching ratio is consistent with some results, none of the calculations is in good agreement with all measured weak radiative decay parameters. As we will show below, this conclusion remains unchanged, especially since over the last few years the first measurements of branching ratios and asymmetries for $\Xi^0 \to \Lambda\gamma$ [43] and $\Xi^0 \to \Sigma^0\gamma$ [44] have appeared.

Two of the most recent theoretical calculations involving all weak radiative hyperon decays are Uppal and Verma [35] and Żenczykowski [24]. Both calculations fail to accommodate our result, giving 0.69×10^{-3} and 1.0×10^{-3}, respectively. Maity and Mahato [29] unfortunately did not include the decay $\Lambda \to n\gamma$. It is interesting to note that Żenczykowski's reanalysis [24] agrees quite well with all the other measured branching ratios. The same is not true for Uppal and Verma [35], nor for Maity and Mahato [29].

Now that we have combined our four measurements, we can also compare our final result, as well as the other recent experimental data, with those theoretical calculations that do agree within errors with our result. This is summarized in Table II. With the possible exception of Żenczykowski's most recent fits [47] all of these calculations fail to reproduce some of the other experimental results. Because of strong cancellations in the parity-conserving amplitudes, Żenczykowski's fits can accommodate our present result if the experimental uncertainty in the $\mu(\Sigma\Lambda)$ transition magnetic moment is taken into account. There is a potential problem with the sign of the asymmetry for $\Xi^0 \to \Sigma^0\gamma$ (see Table II); however, the experimental error on this is quite large. A crucial test for this theoretical approach is the asymmetry for $\Xi^- \to \Sigma^-\gamma$. It is predicted to be around $+0.6$, and we look forward to first results from Fermilab E761 [48].

In conclusion then, our much improved and more reliable branching ratio for $\Lambda \to n\gamma$ should be used as a new incentive for improved theoretical calculations.

TABLE II. Theoretical calculations agreeing with our branching ratio for $\Lambda \to n\gamma$ of $(1.75 \pm 0.15) \times 10^{-3}$. Column 3 shows those predictions for branching ratios and asymmetry parameters that fail to agree with experimental information. All branching ratios are in units of 10^{-3}.

Reference	Theoretical B for $\Lambda \to n\gamma$	Other theoretical predictions	Corresponding experimental values
Verma, 1990 [31]	1.62	$B(\Xi^0 \to \Lambda\gamma) = 0.5$	1.06±0.16
		$\alpha_\gamma(\Xi^0 \to \Sigma^0\gamma) = -0.94$	0.2±0.32
Liu, 1989 [29]	1.73	$B(\Xi^0 \to \Sigma^0\gamma) = 0.23$	3.56±0.43
		$\alpha_\gamma(\Xi^0 \to \Lambda\gamma) = -1.0$	0.43±0.44
Verma and Sharma, 1988 [31]	1.66	$B(\Xi^0 \to \Lambda\gamma) = 0.57$	1.06±0.16
		$\alpha_\gamma(\Xi^0 \to \Sigma^0\gamma) = 0.81$	0.2±0.32
Kamal and Verma, 1982 [45]	1.70	$B(\Xi^0 \to \Sigma^0\gamma) = 0.23$	3.56±0.43
		$B(\Xi^- \to \Sigma^-\gamma) = 1.20$	0.23±0.1
Scadron and Thebaud, 1973 [46]	1.50	$B(\Xi^0 \to \Lambda\gamma) = 15.0$	1.06±0.16
		$B(\Xi^0 \to \Sigma^0\gamma) = 10.0$	3.56±0.43
Żenczykowski, 1992 [47]	1.61	$\alpha_\gamma(\Xi^0 \to \Sigma^0\gamma) = -0.36$	0.2±0.32

B. The radiative capture $K^- p \to \Sigma(1385)\gamma$

Our initial interest in this reaction was partially aroused by the very interesting prediction of Düsedau and Jaffe [14] that polarized Λ hyperons might be produced in the decay of kaonic hydrogen. Radiative capture to the $\Sigma(1385)$ would play an important role in this production of polarized Λ hyperons. During the data analysis it became clear that we did not have the statistical sensitivity to successfully look for this effect. Therefore we focused our effort on just the branching ratio for this radiative capture reaction.

There are two reasons why this process is expected to have a lower branching ratio than the other two rather similar processes that have been measured, $K^- p \to \Lambda\gamma$ and $K^- p \to \Sigma^0\gamma$. These are the following

(i) The γ energy is about 47 MeV, which is much lower than for $K^- p \to \Lambda\gamma$ ($E_\gamma = 282$ MeV) or $K^- p \to \Sigma^0\gamma$ ($E_\gamma = 219$ MeV). Since the transition rates are proportional to E_γ^3, this is expected to reduce the branching ratio for $K^- p \to \Sigma(1385)\gamma$ by about 2 orders of magnitude.

(ii) The Kp system at rest is known to be strongly influenced by the $\Lambda(1405)$, which has a mass close to that of the Kp system (1432 MeV). Thus the branching ratio for $K^- p \to \Sigma(1385)\gamma$ is expected to be related to the radiative decay width for $\Lambda(1405) \to \Sigma(1385)\gamma$. Two calculations of this radiative decay width have been published [49,50] and a third is in progress [51]. Both of the published calculations are based on the Isgur-Karl model, and both predict a radiative width for $K^- p \to \Sigma(1385)\gamma$ much lower than for $\Lambda(1405) \to \Lambda\gamma$ or $\Sigma^0\gamma$.

The second of these reasons is model dependent, and it will be interesting to see if the different approach used by Umino and Myhrer [21,51] shows the same trend as the Isgur-Karl model calculations. However, the first point is essentially model independent and, since the branching ratios for $K^- p \to \Lambda\gamma$ and $\Sigma^0\gamma$ are around 10^{-3}, it is expected that the branching ratio for $K^- p \to \Sigma(1385)\gamma$ will not exceed about 10^{-5}. Thus, the present upper limit of 4×10^{-4} is not unexpected but serves to preclude any unanticipated strong enhancement for this transition.

ACKNOWLEDGMENTS

We wish to thank R. K. Adair and the Brookhaven National Laboratory management for their financial support for the transfer of the Crystal Box from LAMPF to BNL. We wish to thank H. Georgi, R. L. Jaffe, P. Singer, and P. Żenczykowski for helpful discussions and correspondence on the theory. We are grateful to N. P. Hessey for contributions during the design stage of the experiment. We would also like to thank the staff of Brookhaven National Laboratory for the provision of facilities, and especially R. Meier for construction and maintenance of the hydrogen target. We are grateful to C. M. Hoffman and G. Garvey for the loan of the Crystal Box. This work was supported by the U.S. Department of Energy, the National Science Foundation, the U.K. Science and Engineering Research Council (SERC) and the Canadian National Science and Engineering Research Council (NSERC).

[1] L. K. Gershwin *et al.*, Phys. Rev. **188**, 2077 (1969).
[2] A. Manz *et al.*, Phys. Lett. **96B**, 217 (1980).
[3] M. Kobayashi, J. Haba, T. Homma, H. Kawai, K. Miyake, T. S. Nakamura, N. Sasao, and Y. Sugimoto, Phys. Rev. Lett. **59**, 868 (1987).
[4] M. Foucher *et al.*, Phys. Rev. Lett. **68**, 3004 (1992).
[5] S. F. Biagi *et al.*, Z. Phys. C **30**, 201 (1986).
[6] N. P. Hessey *et al.*, Z. Phys. C **42**, 175 (1989).
[7] N. P. Hessey, Ph.D. thesis, University of Birmingham, 1988.
[8] D. A. Whitehouse *et al.*, Phys. Rev. Lett. **63**, 1352 (1989).
[9] K. P. Gall *et al.*, Phys. Rev. C **42**, R475 (1990).
[10] D. A. Whitehouse, Ph.D. thesis, Boston University, 1989.
[11] K. P. Gall, Ph.D. thesis, Boston University, 1989.
[12] D. J. Miller, R. J. Nowak, and T. Tymieniecka, in *Proceedings of the International Conference on Low and Intermediate-Energy Kaon-Nucleon Physics,* edited by E. Ferrari and G. Violini (Reidel, Dordrecht, 1980), p. 251.
[13] Particle Data Group, J. J. Hernández *et al.*, Phys. Lett. B **239**, 1 (1990).

[14] D. W. Düsedau and R. L. Jaffe, Phys. Lett. B **186**, 425 (1987).
[15] H. Burkhardt, J. Lowe, and A. S. Rosenthal, Nucl. Phys. **A440**, 653 (1985).
[16] J. W. Darewych, R. Koniuk, and N. Isgur, Phys. Rev. **32**, 1765 (1986).
[17] R. L. Workman and H. Fearing, Phys. Rev. D **37**, 3117 (1988).
[18] H. Burkhardt and J. Lowe, Phys. Rev. C **44**, 607 (1991).
[19] J. Lowe, in *Proceedings of the International Symposium on Hypernuclear and Low-Energy Kaon Physics,* Padova, Italy, 1988, edited by T. Bressani, F. Cannata, J. Lowe, and R. A. Ricci [Nuovo Cimento A **102**, 167 (1989)].
[20] R. H. Dalitz and J. G. McGinley, in *Proceedings of the International Conference on Low and Intermediate-Energy Kaon-Nucleon Physics* [12], p. 381.
[21] Y. Umino and F. Myhrer, Nucl. Phys. **A529**, 713 (1991).
[22] A. J. Noble *et al.*, Phys. Rev. Lett. **69**, 414 (1992).
[23] Y. Hara, Phys. Rev. Lett. **12**, 378 (1964).
[24] P. Żenczykowski, Phys. Rev. D **44**, 1485 (1991).
[25] R. E. Karlsen, W. H. Ryan, and M. D. Scadron, Phys. Rev. D **43**, 157 (1991).
[26] P. Singer, Phys. Rev. D **42**, 3255 (1990); D. Palle, *ibid.* **36**, 2863 (1987).
[27] P. Asthana and A. N. Kamal, Few Body Sys. **11**, 1 (1991).
[28] I. I. Balitsky, V. M. Braun, and A. V. Kolesnichenko, Nucl. Phys. **B312**, 509 (1989); C. Goldman and C. O. Escobar, Phys. Rev. D **40**, 106 (1989).
[29] Y. Liu, Z. Phys. C **45**, 345 (1989); G. Nardulli, Nuovo Cimento A **100**, 485 (1988); R. E. Karlsen and M. D. Scadron, Z. Phys. C **52**, 325 (1991); A. Maity and P. Mahato, Nuovo Cimento A **104**, 269 (1991); M. B. Gavela, A. Le Yaouanc, L. Oliver, O. Pène, J. C. Raynal, and T. N. Pham, Phys. Lett. **101B**, 417 (1981).
[30] R. W. Brown and E. A. Paschos, Nucl. Phys. **B319**, 623 (1989); M. D. Scadron and M. Visinescu, Phys. Rev. D **28**, 1117 (1983).
[31] R. C. Verma and A. Sharma, Phys. Rev. D **38**, 1443 (1988); in *The Standard Model and Beyond,* Proceedings of the 5th Winter Institute, Lake Louise, Canada, 1990, edited by A. Astbury *et al.* (World Scientific, Singapore, 1990), p. 390; F. J. Gilman and M. B. Wise, Phys. Rev. D **19**, 976 (1979); R. Safadi and P. Singer, *ibid.* **37**, 697 (1988); L. Bergström and P. Singer, Phys. Lett. **169B**, 297 (1986).
[32] W. F. Kao and H. J. Schnitzer, Phys. Rev. D **37**, 1912 (1988).
[33] M. K. Gaillard, X. Q. Li, and S. Rudaz, Phys. Lett. **158B**, 158 (1985).
[34] L. Chong-Huah, Phys. Rev. D **26**, 199 (1982).
[35] T. Uppal and R. C. Verma, Z. Phys. C **52**, 307 (1991).
[36] B. Bassalleck, Nucl. Phys. **A547**, 299c (1992).
[37] S. L. Wilson *et al.*, Nucl. Instrum. Methods A **264**, 263 (1988).
[38] S. L. Wilson, Los Alamos National Laboratory Report No. LA-10471-T, 1985 (unpublished).
[39] K. D. Larson, Ph.D. thesis, University of New Mexico, 1990.
[40] A. J. Noble, Ph.D. thesis, University of British Columbia, 1990.
[41] R.Brun *et al.*, CERN Report No. DD/EE/**84-1**, 1987 (unpublished); H. C. Fesefeldt, Physikalisches Institut der Technischen Hochschule Aachen (PITHA) Report No. **84-02**, 1985 (unpublished).
[42] A. D. Martin, Nucl. Phys. **B179**, 33 (1981).
[43] C. James *et al.*, Phys. Rev. Lett. **64**, 843 (1990).
[44] S. Teige *et al.*, Phys. Rev. Lett. **63**, 2717 (1989).
[45] A. N. Kamal and R.C. Verma, Phys. Rev. D **26**, 190 (1982).
[46] M. D. Scadron and L.R. Thebaud, Phys. Rev. D **8**, 2190 (1973).
[47] P. Żenczykowski (private communication).
[48] M. Foucher (private communication).
[49] J. W. Darewych, M. Horbatsch, and R. Koniuk, Phys. Rev. D **28**, 1125 (1983).
[50] E. Kaxiras, E. J. Moniz, and M. Soyeur, Phys. Rev. D **32**, 695 (1985).
[51] Y. Umino (unpublished).